Surface & Coatings Technology 383 (2020) 125251

Contents lists available at ScienceDirect

Surface & Coatings Technology

journal homepage: www.elsevier.com/locate/surfcoat

Characterization of the cold spray deposition of a wide variety of polymeric powders

Zahra Khalkhali, Jonathan P. Rothstein*

Department of Mechanical and Industrial Engineering, University of Massachusetts, Amherst, MA 01003, USA

ARTICLE INFO

Keywords:
Cold spray
Polymer powders
Deposition window
Deposition efficiency
Adhesion/cohesion strength

ABSTRACT

The cold spray deposition of high-density polyethylene, polyurethane, polystyrene, polyamide 12, and ultrahigh molecular weight polyethylene on a variety of polymeric substrates was studied. A variety of different process conditions were studied in order to develop deposition windows over temperature-velocity space for each particle/substrate combination. The deposition windows for each polymer powder were shown to expand as the particle and substrate temperatures were increased. In general, lower glass transition temperature materials were found to deposit more easily and with larger deposition efficiency. Nano-indentation and adhesive/cohesive strength experiments were conducted on the cold sprayed samples and the results were found to be statistically identical to those of corresponding melt-cast samples. Microstructural characterization showed little to no porosity in the deposited polymer films. Finally, deposition efficiency was studied as a function of the tilt angle of the substrate to better understand potential of this technology for additive manufacturing three-dimensional components. A critical tilt angle was found above which successful deposition was not possible. This critical tilt angle was found to increase with increasing impact velocity.

1. Introduction

Since the first application of cold spray as a coating technique more than 30 years ago [1], there have been a wide array of studies on use of the cold spray process for depositing a variety of powder particles including metals, polymers, composites, and ceramics on various substrates [1,2]. Cold spray utilizes a preheated high-pressure gas flow to accelerate the desired particles to high speeds through a Laval converging-diverging nozzle. Upon impact on a substrate, the powder particles can deposit to form a uniform non-porous coating. The bond that forms between the particle and substrate can be metallurgical, chemical, and/or mechanical and results from the severe plastic deformation of the particle and the substrate during the high kinetic energy impact [3–6].

In the cold spray process, the sprayed particles remain in their solid state during the entire deposition process minimizing the chance of oxidation, degradation, residual stresses and any other defects associated with high temperature coating processes [7,8]. Microstructural mismatches and stresses resulting from thermal expansions and contractions during processing are also minimized in this technique [3,4]. Finally, as no solvent is used, cold spray is considered to be a green additive manufacturing process. As a result of all these inherent advantages, the cold spray process is currently being implemented in an number of applications areas including: the aerospace industry [9–12], biomaterials [13–15], photocatalysts [16], copper-based catalysts [17] antifouling surfaces [18,19], antibacterial coatings [2,13], renewable energy [20] and epoxy-based powder coatings as a promising alternative to solvent-borne coatings [21].

A number of bonding mechanisms for the cold spray deposition of metallic powders have been proposed over the past 20 years [22]. Most proposed bonding mechanisms require, to some degree, that during particle impact, plastic strain energy is released locally as heat to soften the material and encourage further deformation and heat release [23]. This positive feedback condition is known as the adiabatic shear instability and it occurs at high strain rates where the rate of thermal softening within the impacting particle or the substrate exceeds the rates of strain and strain-rate hardening [23]. These high deformation rates can lead to interfacial flow instability [24] that can promote mechanical interlocking between the particle and the substrate [25], crack filling [26] and the formation of metallic bonds between the particle and the substrate once the oxide layer has been stripped during impact [23]. In a recent study, Hassani-Gangaraj et al., argued that adiabatic shear instability is not necessary for adhesion in cold spray. They found that hydrodynamic plasticity, which is a natural dynamic effect in high-speed impacts, is enough to create the bond at the particle/substrate interface. They assigned the hydrodynamic plasticity to

* Corresponding author.
E-mail address: rothstein@ecs.umass.edu (J.P. Rothstein).

https://doi.org/10.1016/j.surfcoat.2019.125251
Received 9 September 2019; Received in revised form 6 December 2019; Accepted 10 December 2019
Available online 12 December 2019

Table 1
Material properties of the feedstock powders.

Materials	T_g (°C)	T_m(°C)	D (μm)	Yield Strength [MPa]	Density [kg/m^3]	Source
HDPE	−90	128	48 ± 18	20	990	BYK Ceraflour
Polyurethane	−63	92	50 ± 11	24	985	KU Leuven
Polyamide 12	97	180	50 ± 25	50	1010	KU Leuven
Polystyrene	100	175	44 ± 4	34	1040	KU Leuven
UHMWPE	−150	130	20 ± 7	22	949	Mipelon ™

the interaction of strong pressure waves with the free surface at the particle edges [27]. All of these phenomena can aid particle adhesion, although for polymeric particles, due to the lack of metallic bonds, mechanical interlocking is the most likely bonding mechanism.

Cold spray has also been studied for polymeric materials although less broadly than metals [3,4,13,28,29,30]. Due to the differences in mechanical properties, thermal conductivity, availability of metallic bonds, and the degree of crystallinity, the polymer particles behave significantly different from metals during the whole cold spray process [3,29]. Xu et al. [29] reported a critical velocity of 100 m/s and a deposition efficiency < 0.5% for the 150–250 μm High-density polyethylene (HDPE) particles on an HDPE sheet. Alhulaifi et al. [31] studied smaller HDPE particles (D = 53–75 μm) cold sprayed on an aluminum substrate using a diffuser nozzle to reduce the particle velocity and reported a critical velocity of 190 m/s. Bush et al. [3] systematically studied the effect of particle size, velocity, temperature and nozzle design the deposition efficiency and deposition window of HDPE particles. They formed dense and uniform coatings of HDPE particles on a variety of polymeric substrates yielding deposition efficiencies of close to 10% of HDPE particles on soft LDPE substrates and slightly lower efficiencies on other substrates. They highlighted that the empirical formula used to determine the critical impact velocity for the cold spray deposition of metallic particles on metal substrates can be applied to polymeric particles. However the empirical fitting constant was found to be three times smaller than that of metallic particles resulting in deposition at significantly smaller velocities [3]. Shah et al. [30] incorporated finite element simulation studies of cold spray deposition of HDPE particles on a variety of polymeric and non-polymeric substrates. They showed that increasing the kinetic energy or the particle or the mismatch in modulus between the impacting polymer particle and the substrate increased the likelihood of deposition by increasing the plastic deformation and the localized heating in the region of impact.

A number of studies have investigated composite polymer particles. Ravi et al. [32] studied cold spray deposition of ultra-high molecular weight polyethylene (UHMWPE) onto both aluminum and polypropylene substrates. They added up to 4 wt% of alumina nanoparticles to increase the particle density and facilitate inter-particle bonding through topochemical reactions. Without the addition of the nanoparticle, Ravi et al. [32] were unsuccessful in their attempts to cold spray UHMWPE. Gillet et al. [33] studied the cold spray deposition of copper coated PEEK (Poly-Ether-Ether-Ketone) particles reinforced by carbon fibers within the PEEK. They found deposition impossible without the addition of a thin layer of pure PEEK to the outer surface of the particle. Yang et al. [21] studied the deposition of a series polymeric particles with a core-shell structure containing epoxy resin and poly (methyl methacrylate) on an aluminum substrate using a laser induced single particle impact experiment designed to mimic the cold spray process. They showed that the critical velocity for particle deposition was decreased significantly when the glass transition temperature of the polymer core was decreased to promote plastic deformation upon impact on the substrate [21]. In this paper, we study the impact that changing the glass transition temperature can have on the cold spray deposition of homopolymer powders.

The inherent roughness of the substrate and the angle made between the cold spray nozzle and the features built up on the substrate can affect the ability to successfully deposit particles. Wang et al. [34] studied the effect of the spray angles on the bond strength of the cold spray deposited particles and the substrate for aluminum particles on an aluminum substrate. They found that the bonding strength increased with decreasing spray angle from the 90° (normal to the substrate) to 45°. However, the deposition efficiency and strength of the bulk deposit material was found to decrease with decreasing spray angle [34]. In the present work, the effect of spray angle on the cold spray deposition of polymer powders was studied to better understand the effect of surface roughness on deposition efficiency and quality. From this work, insights into the bonding mechanism for polymer powders were gained, paths towards improving deposition efficiency of polymeric particles were postulated, and the potential of the cold spray process as a new technique for 3D printing of polymers was illustrated.

The principle objective of this work is to develop window of deposition maps over velocity and particle temperature space and to optimize the conditions for efficient cold spray deposition for a wide variety of polymeric powders including polyurethane, polystyrene, polyamide 12, and ultrahigh molecular weight polyethylene on a variety of polymeric substrates. For each polymer/substrate combination, the microstructural and mechanical properties of the cold spray deposited layers were characterized using scanning electron microscopy, nano-indentation tests, and cohesion/adhesion strength experiments.

2. Materials and methods

In Table 1, the physical dimensions and the typical materials properties from the literature and the manufacturer are provided for the polymer particles studied here. These powder particles included: high density polyethylene (HDPE), polyurethane (PU), polyamide-12 (PA), polystyrene (PS) and ultra-high molecular weight polyethylene (UHMWPE). Each of these polymers has a different molecular architecture that leads to variation in density, Young's modulus, yield strength, melt temperature and glass transition temperature amongst other properties. All the particles used had roughly the same average diameter of D = 50 μm, with the exception of UHMWPE, which had a diameter of D = 20 μm. The particles were, however, very different in shape as can be clearly seen in the SEM images in Fig. 1. Some particles like PS were quite spherical, while many other particles like PU, which were formed through cryo-milling and kindly provided by our colleagues at KU Leuven, were shaped more like flat disks. Although it is not clear from our work whether the shape of the particles affected deposition, the shape of the particles did have a significant impact on the ability to provide a uniform flux of particles from the hopper. The flowability of spherical particles made them easier to work with than the disk-shaped particles [35]. As a consequence, it was possible to process spherical particles at much higher temperatures than disk-shaped particles. Disk-shaped particles became tacky and clogged the hopper at temperatures well below their melt temperature.

Cold-spray deposition of the powder particles was studied on a series of both polymeric substrate materials. These include: high density polyethylene (HDPE) (Vycom Hitec, hardness, Shore Durometer 68 D), polyvinylchloride (PVC) (Vycom Vintec 1, hardness, Shore Durometer 89 D, T_g = 85 °C, T_m = 240 °C), polyoxymethylene (POM) (Quadrant Acetron GP Acetal, hardness, Shore Durometer 85 D, T_g = −60 °C,

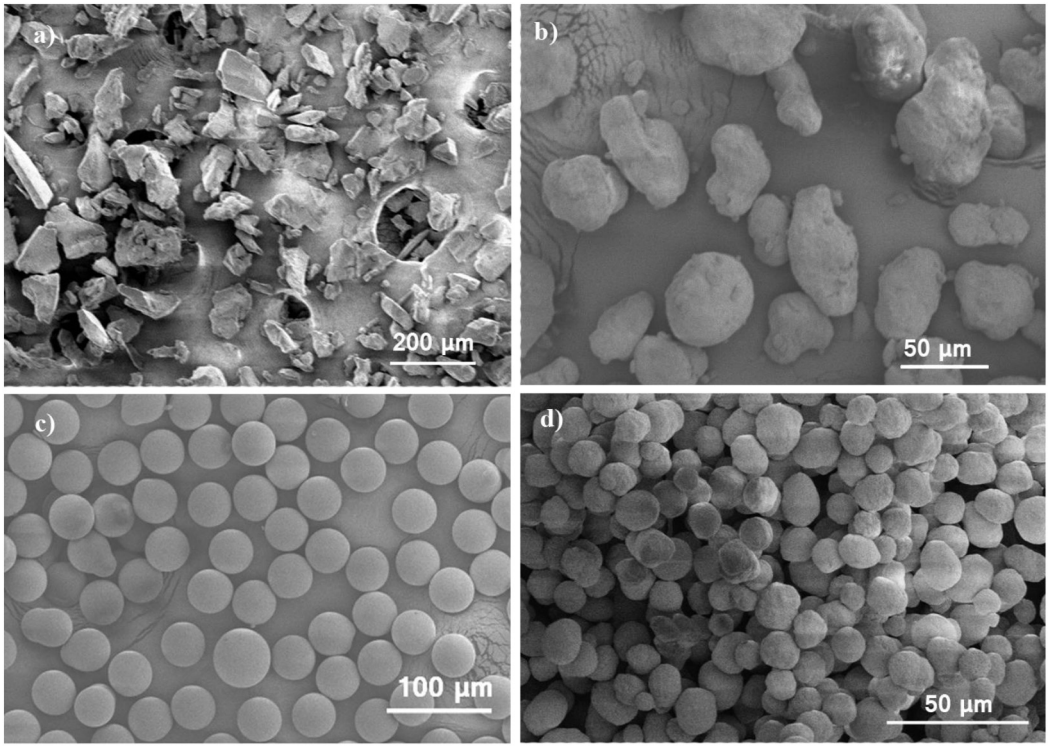

Fig. 1. – SEM imaging of the feedstock powder particles (a) PU, (b) PA, (c) PS and (d) UHMWPE.

T_m = 175 °C), low density polyethylene (LDPE) (McMaster-Carr, hardness, Shore Durometer 45 D, T_m = 110 °C, and T_g = −90 °C) and melt-cast samples of each of the studied materials.

A laboratory-scale cold spray system using a consumer grade single-stage air compressor with the capability of accelerating particles up to Mach 2 (two times the speed of sound) was used to deposit the polymeric particles [3]. This polymer cold spray system can be operated either using a compressed nitrogen cylinder or a consumer-grade single-stage air compressor capable of producing a pressure of 6.2 bars at 8.5 m^3/h. The compressed air traveled through filters and a pressure regulator before entering a heated pressure vessel that housed the powder feeder. The hot gas/powder mixture then exited the vessel and passed through the nozzle. The powder and process gas were heated together and mixed well upstream of the nozzle. The aluminum pressure vessel was heated with three 500 W band heaters (Omega MB-1). The temperature of the pressure vessel was monitored with an internal bore thermocouple (Omega BT) inserted through a radial pressure fitting near the bottom of the barrel and was controlled with a PID temperature controller (Omega CN2110). The inner diameter of the pressure vessel was 38 mm and it had a total length 27 cm. Nozzle inlet conditions were monitored via a thermocouple and a pressure transducer (Omega PX309-300GV) inserted just upstream of the nozzle. A schematic diagram and the complete details of the design of this setup can be found in our previous study [3]. Powder feed was accomplished by routing the carrier air around a vibratory powder dispenser contained in the pressure vessel. A pneumatic vibrator (Cleveland Vibrators VM-25) was mounted on a connecting rod above the pressure vessel. The connecting rod ran through a slip-fit bushing and into the vessel, where it transmitted vibration to an attached aluminum tube that contained the powder to be deposited. The bottom of the tube was capped with coarse wire mesh, which allowed agitated powder to fall into the surrounding carrier gas.

A temperature-controlled two-dimensional (2D) xy-stage operated by an open source software package designed for three-dimensional (3D) printing (Repetier-Host) was used to move the substrate underneath the nozzle exit at controlled speeds to create deposition patterns consisting of one-dimensional (1D) lines and 2D square patterns. The stage could maintain a temperature of up to T = 100 °C during deposition. Here, all 2D deposition patterns were 2 cm × 2 cm squares. These patterns required multiple passes to deposit and used 25% overlap between sequential lines to produce a uniform and flat pattern. The overlap percentage was optimized for specific conditions of particle size, velocity and flowrate. Specifically, D = 50 µm particles traveling at V_i = 150 and with a powder feed of $\dot{m}_p$ = 35 g/min.

A one-dimensional (1D) inviscid model of gas and particle dynamics was used to calculate the velocity, temperature, and pressure variations through the nozzle [36,37]. This model assumes that the particles do not disturb the flow field, but are acted on by the surrounding gas with drag coefficient based on their size and gas velocity and a heat transfer coefficient based on their velocity. The velocity and temperature evolution for the mean particle size was calculated as a function of position along the converging-diverging Laval nozzle to determine the impact temperature and velocity of each polymer powder. For simplicity, the powders were assumed to be a constant diameter sphere which is clearly not always the case, and the temperature was assumed to be uniform across their cross-section or that they are Lumped. Both of these assumptions and the errors they introduce are discussed in detail in Bush et al. [3]. In the data that follows, the errors from these assumptions are incorporated into uncertainty reported for the average values for velocity and temperature presented here. The largest errors were incurred for the particles with the largest polydispersity in size.

Windows of deposition were developed over the temperature velocity space for each powder/substrate combinations. Particle temperature was varied from room temperature up to 120 °C, while the particle velocity was increased from over 50 to 400 m/s. For most polymers, deposition was achieved at subsonic speeds, $Ma < 1$. However, as we will show later, for some systems like UHMWPE, supersonic speeds, $Ma > 1$, were needed to achieve deposition. This required the use of a different nozzle. Whereas all the subsonic were performed using a nozzle with only a converging section, the supersonic tests used a converging-diverging nozzle documented in Bush et al. [3].

Imaging of both coating surface and cross-section was performed on

a FEI Magellan 400 XHR-SEM with nanometer resolution. To prepare the cold sprayed samples for the cross-sectional studies, the depositions were applied on the edge rather than the middle of the substrate. The other sides were cut using forged steel scissors but only the un-cut edge was studied by the SEM. To ensure accurate void identification, three images were taken at slightly different angles and then were compared with each other. Surface hardness measurements were performed using a nano-indentation instrument. Specifically, a Hysitron piezo controller IV-A equipped with a standard Berkovich indenter with a 300 nm three-sided pyramidal tip and a maximum displacement range of 2 mm was used. The displacement resolution and the loading resolution were 0.01 nm and 50 nN, respectively. The maximum testing load was 50 μN and the indentation depths were within 10% of the coatings' thickness, thus minimizing substrate effects. All samples were 1 mm thick cold spray coating on 2 mm thick LDPE substrates. All samples were first ground mechanically using SiC sandpaper to ensure a smooth surface. The loading and its corresponding displacement were recorded as a function of time during the experiment. The surface hardness of cold sprayed surfaces was compared to that of a melt cast sample of that polymer material serving as the 'bulk' material reference. The small scale of nano-indentation allows a spatial map of hardness to be generated. Knowledge of spatial variation in hardness is important to understand the uniformity of the coating. About 20 measurements were made over an area of 4 mm^2 to determine the uniformity of surface properties.

Adhesion strength was measured according to ASTM-C633 standard [38] that is generally used to measure the adhesion strength of both thermal sprayed and cold sprayed samples [39]. The tests are based on linear elastic fracture mechanics approach, and consist of subjecting an assembly of coating, substrate and fixtures to a tensile load (normal to the plane of the coating). Melt cast specimens of each of the five polymer materials were prepared using a vacuum hot press machine to ensure removal of the voids from the melt. Rectangular prisms with dimensions 2 mm × 5 mm × 5 mm were cut out of the melt cast samples and used as substrates. Polymer powders were deposited onto corresponding melt-cast samples using cold-spray to create 2 mm thick deposition on the substrates. Thickness of the coatings was adjusted by the traverse speed. An epoxy (polyamide-epoxy FM 1000) was then used to glue the coating/substrate pairs between the two halves of a dog-bone sample of melt-cast polyamide 12 as shown in Fig. 2. The dog bone samples were left for 16 h at room temperature for the epoxy to fully be cured and trimmed to ensure a constant thickness along the dog bone.

A Servo-hydraulic Dartec machine with a 20 kN load cell connected to an Instron controller was employed to carry out the tests at room temperature, $T = 20$ °C. The dog bone specimens were clamped at both ends. One end was fixed while the other was displaced at a pre-defined

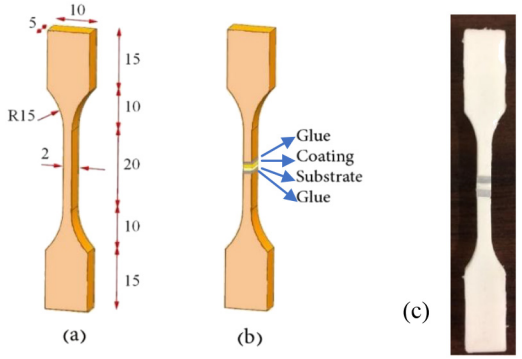

Fig. 2. – (a) Dimensions of the standard polyamide 12 dog bone used for the adhesion/cohesion strength testing, (b) schematic diagram of how the coating/substrate were glued into the dog bone, (c) example of a dog bone before testing.

velocity of 0.033 mm/s, which corresponds to an initial strain rate of $10^{-3}\,s^{-1}$. The length, width and thickness of all specimens were measured with a sliding caliper prior to the testing. The force-displacement curves were converted to stress-strain curves for each testing after dividing the force by the cross-sectional area and dividing the displacement by the initial length of the samples. A minimum of three tests were performed for specimens of each polymer material, and the resulted curves were compared to ensure repeatability of the results.

3. Results and discussion

3.1. Windows of deposition

3.1.1. High density polyethylene

Cold spray deposition of HDPE powders was studied on four different polymeric substrates including LDPE, HDPE, POM and PVC. A material-dependent window of deposition was determined for each substrate as a function of particle temperature and particle impact velocity. The critical velocity above which deposition was observed, was found to be between 50 and 100 m/s for HDPE particles cold sprayed on the various substrates. Like metallic cold spray, the critical velocity was found to decrease with increasing the particle temperature, however, it was at least three times less than the prediction of the empirical method used in metallic cold spray which yields a critical velocity of between 300 and 400 m/s. The details of the study are found in [3].

3.1.2. Polyurethane

In Fig. 3, the deposition windows of PU on a variety of substrates including LDPE, PU, PVC, and POM are shown. The substrate temperature was fixed at $T_s = 100$ °C. Substrates were attached on top of a heated bed on a moving stage. The temperature of the printed circuit board (PCB) bed was monitored by an embedded thermistor and was controlled by the RAMPS system ((RepRap Arduino Mega Pololu Shield). Therefore, the fixed temperature of $T_s = 100$ °C refers to the bed temperature on which the substrate was attached. The particle flowrate was kept between 45 and 55 g/min in all experiments. The critical impact velocity was found to decrease with increasing particle temperature. For the case of deposition on LDPE for instance, a reduction in the critical impact velocity for adhesion from $V_{cr} = 100$ m/s at $T_p = 20$ °C to $V_{cr} = 90$ m/s at $T_p = 80$ °C can be seen in Fig. 3. These results are consistent with our previous cold spray results for HDPE particles deposited on LDPE [3]. As was seen in Bush et al. [3], based on the critical velocity equation of Schmidt et al. [40], the critical velocity for successful deposition of PU was a factor of four or five times smaller than what would be predicted for metal particles with similar mechanical properties. As a result, deposition is possible even at relatively low particle velocities far from the speed of sound and the detrimental effects of shock waves.

Like-on-like deposition of PU powders on a melt cast PU substrate was found to be more difficult than deposition on LDPE. For deposition on PU substrates, the critical velocity for adhesion shifted to larger velocities especially at lower temperatures. For example, at room temperature, $T_p = 20$ °C, the critical impact velocity for adhesion increased from $V_{cr} = 100$ m/s on LDPE to $V_{cr} = 135$ m/s on PU. Like-on-like deposition of PU was also found to be more sensitive to particle temperature than deposition on LDPE. Here, the critical impact velocity for adhesion drops to $V_{cr} = 90$ m/s at a particle temperature of $T_p = 80$ °C. This is most likely because, in the case of deposition of particles on LDPE, most of the deformation takes place in the soft substrate which is not changing with particle temperature. While for like-on-like deposition, much of the deformation needed for adhesion occurs within the impacting particle, which gets softer and more mobile as the temperature approaches its melt temperature, T_{melt}. Deposition of PU particles on the harder POM and PVC substrates were similar to like-on-like deposition on PU. The main difference was that the PU particles were found to exhibit an upper bound on velocity at which successful

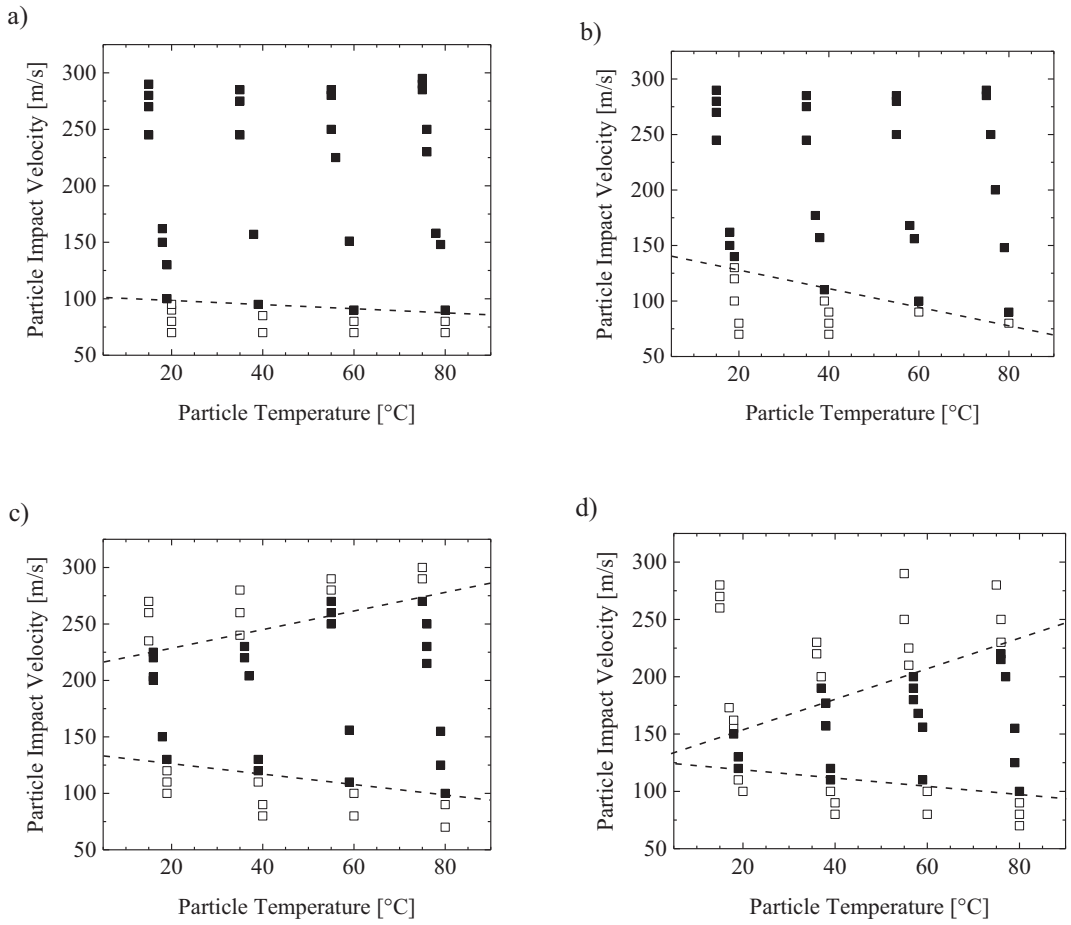

Fig. 3. Cold spray deposition window for PU particles on substrates of (a) LDPE, (b) PU, (c) PVC and (d) POM. Data include experiments showing (■) successful deposition, and (□) no deposition. In all cases, the substrate was held fixed at $T_s = 100\,^{\circ}C$ and the nozzle stand-off distance was 10 mm. The dashed lines are not meant to be quantitative but are simply there to guide the reader's eye.

deposition was possible. Within the studied velocity ranges, deposition was not found to have an upper velocity limit on PU or LDPE. However, on the POM and PVC substrates, it is clearly evident. Above these maximum deposition velocities, deposition was found to fail through an adhesive failure of the deposition after an initial build up. The minimum thickness for deposition was considered to be about 200 μm. For PU deposition on PVC, the upper velocity for successful deposition starts at $V_{cr} = 225$ m/s at $T_p = 20\,^{\circ}C$ and grows with particle temperature to $V_{cr} = 275$ m/s at $T_p = 80\,^{\circ}C$. The deposition window is significantly narrower for PU deposition on POM. These results show that deposition is strongly dependent on the particle/substrate combinations chosen. The upper limit for deposition of polyurethane on POM and PVC was also observed for HDPE particles [3,4].

3.1.3. Polyamide 12

In Fig. 4, the cold spray deposition windows of PA particles on a variety of substrates including LDPE, PA, PVC, and POM are shown. Note that the data in Fig. 4 a) and b) was originally published in [4] and has been replotted here for comparison. Deposition of PA was significantly more difficult than for the PU described in Section 3.1.2. A critical velocity of $V_{cr} = 170$ m/s was required for PA on LDPE and 180 m/s was needed to deposit PA on a melt cast PA at 20 °C. That is nearly a two-fold increase in the critical velocity for PU on LDPE. This large difference is likely due to the increase in the glass transition temperature of the polymer powders. For PU, the glass transition temperature is $T_g = -63\,^{\circ}C$ meaning that, even at room temperature, the amorphous fraction of the PU polymer chains within the particles are quite mobile. In contrast, for PA the glass transition temperature is well above room temperature, $T_g = 97\,^{\circ}C$, and as a result both the amorphous fraction of the PA polymer chains in the particle and the substrate are glassy at all but the highest temperatures tested. Only in the thin region in the impact crater, where the kinetic energy of the particle is transformed into thermal energy, will the temperature rise be large enough for the local polymer temperature to rise significantly above its T_g and begin to flow [30]. As a result, more kinetic energy is needed to initiate sufficient plastic deformation and polymer heating to result in particle adhesion.

Additionally, although deposition on LDPE shows no upper velocity limit, like-on-like deposition for PA showed an upper velocity limit which resulted in a very narrow deposition window especially at the lower temperatures tested. At room temperature, deposition was only possible in a narrow window between 195 and 205 m/s. The deposition map was found to get even narrower in the case of depositing on PVC and POM. PVC has a higher glass transition temperature, $T_g = 85\,^{\circ}C$, than LDPE, $T_g = -110\,^{\circ}C$. POM, on the other hand, has a low glass transition temperature of its amorphous component, $T_g = -60\,^{\circ}C$ [41], it is highly crystalline and, as such, has a high fraction of a rigid phase that remains frozen up to the melting temperature ($T_m = 175\,^{\circ}C$). This melt temperature is well beyond the temperature expected to be achieved during particle impact, thus makes deposition almost impossible at room temperature on POM. The deposition window does, however, expand to between 150 m/s and 225 m/s on PA, PVC, and POM as the particle temperature is increased well above its T_g to 120 °C. Improved results would likely be possible for like-on-like deposition if the substrate temperature could be raised beyond the glass transition temperature as well. Unfortunately, we were limited experimentally to

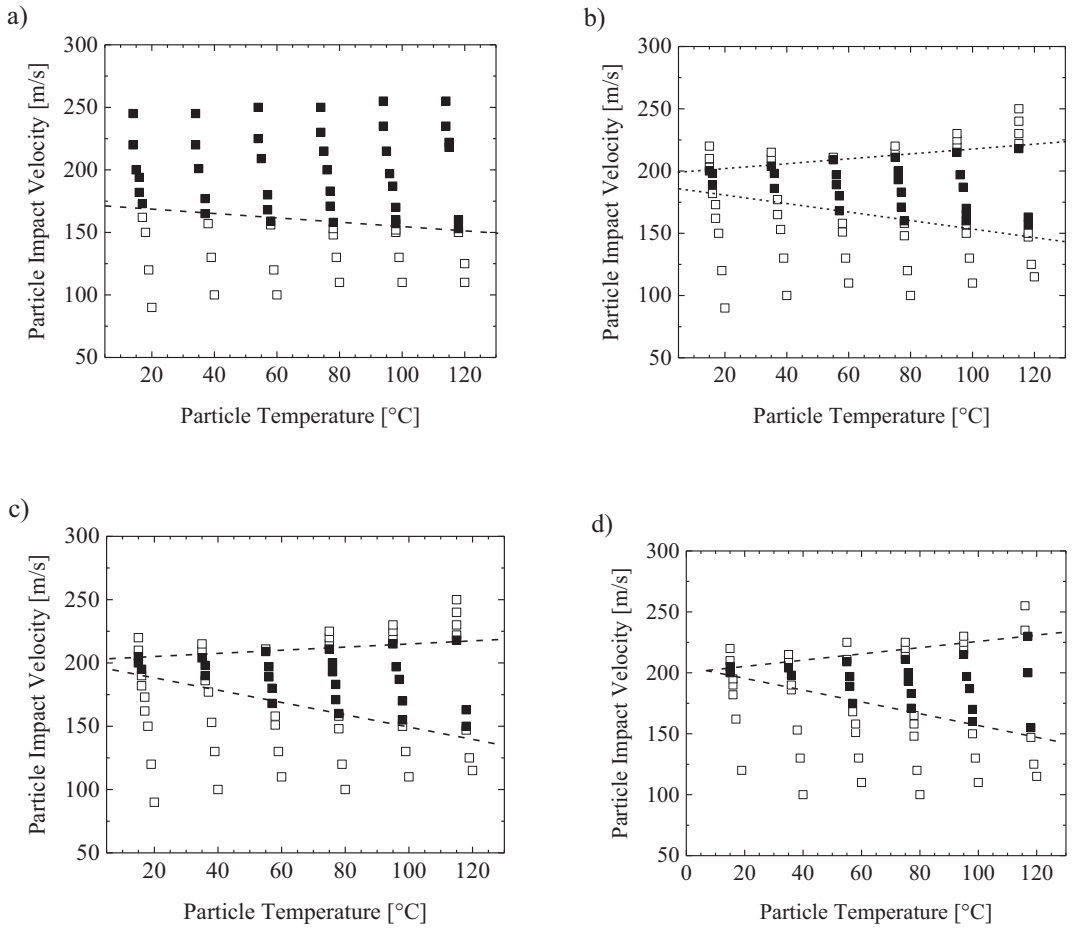

Fig. 4. – Cold spray deposition window of PA particles on (a) LDPE, (b) PA, (c) PVC and (d) POM substrates showing the transition from no deposition (▫) to deposition (▪). In all cases, the substrate was held fixed at T_s = 100 °C and the stand-off distance was 10 mm. The dashed lines are not meant to be quantitative but are simply there to guide the reader's eye.

a maximum substrate temperature of T_S = 100 °C.

3.1.4. Polystyrene

In Fig. 5, the deposition windows of PS on a variety of substrates including LDPE, PS, PVC, and POM are shown. The observations are similar to the results for PA except that an upper velocity limit for.

successful deposition was found to emerge in all cases even for the deposition of PS on LDPE. The effect of substrate was less significant. The deposition was almost twice as wide for PS on LDPE than PS, PVC or POM. Replacing the LDPE substrate with PS, for example, increased the minimum critical velocity for particle adhesion from V_{cr} = 160 m/s to 180 m/s for PS particles and decreased the maximum velocity for particle adhesion from 225 m/s to 215 m/s at room temperature. Note that the data in Fig. 5 a) and b) was originally published in [4] and has been replotted here for comparison.

3.1.5. UHMWPE

UHMWPE is utilized in the applications demanding high wear resistance, high impact resistance and high cavitation erosion resistance. UHMWPE is a comparably efficient (high strength to weight ratio), inexpensive and an easily procurable option to hard alloys and intermetallic compounds which are often used in such applications [42]. In Fig. 6, deposition windows over the particle temperature and particle velocity space are demonstrated for both of the cold spray deposition of UHMWPE particles on an LDPE substrate and deposition of UHMWPE on a melt cast UHMWPE substrate. Deposition windows of UHMWPE on POM and PVC are not presented in Fig. 6 because successful deposition was not achieved. Compared to all the previously studied materials, the deposition window for UHMWPE was found to shift to much larger values of both particle temperatures and particle velocities. On LDPE, deposition of UHMWPE was not possible for particle temperature below T_p = 60 °C. Even beyond 60 °C, an impact velocity of 280 m/s was needed to deposit UHMWPE on LDPE. Compared to HDPE, this is an increase in V_{cr} of > 150 m/s even though the materials have similar melt and glass transition temperatures. The higher molecular weight of the UHMWPE clearly impacts its mobility upon particle impact, reducing the plastic deformation, flow, and mixing between the particle and substrate that is necessary for adhesion. Interestingly, no upper limit was found even as the particles and the carrier gas were accelerated well past the speed of sound. For the case of deposition of UHMWPE on UHMWPE, deposition required particle temperatures above T_p > 80 °C and velocities of at least V_{cr} = 300 m/s. Interestingly, for HDPE, these same impact velocities were found to cause particles to be stripped from the substrate and mild abrasion of the substrate [3].

As the results in Fig. 6 illustrated, deposition of UHMWPE on a low-T_g organic substrate is significantly easier than on a hard, high-T_g polymeric substrate or an inorganic substrate, for that matter. In fact, in the work of Ravi et al. [42], they showed that the deposition of neat UHWMPE on an aluminum substrate was not only feasible even at extremely high temperatures approaching 500 °C as deposition efficiencies of only 0.2% were achieved. Only after the addition of 10% fumed nano-alumina (FNA) particles to the feedstock powder to enhance surface activity of UHMWPE particles and induce chemical bonding with the substrate was a deposition efficiency of > 1% achieved. As will be discussed in Section 3.3, increasing temperature and impact velocity increase the deposition efficiency of the neat

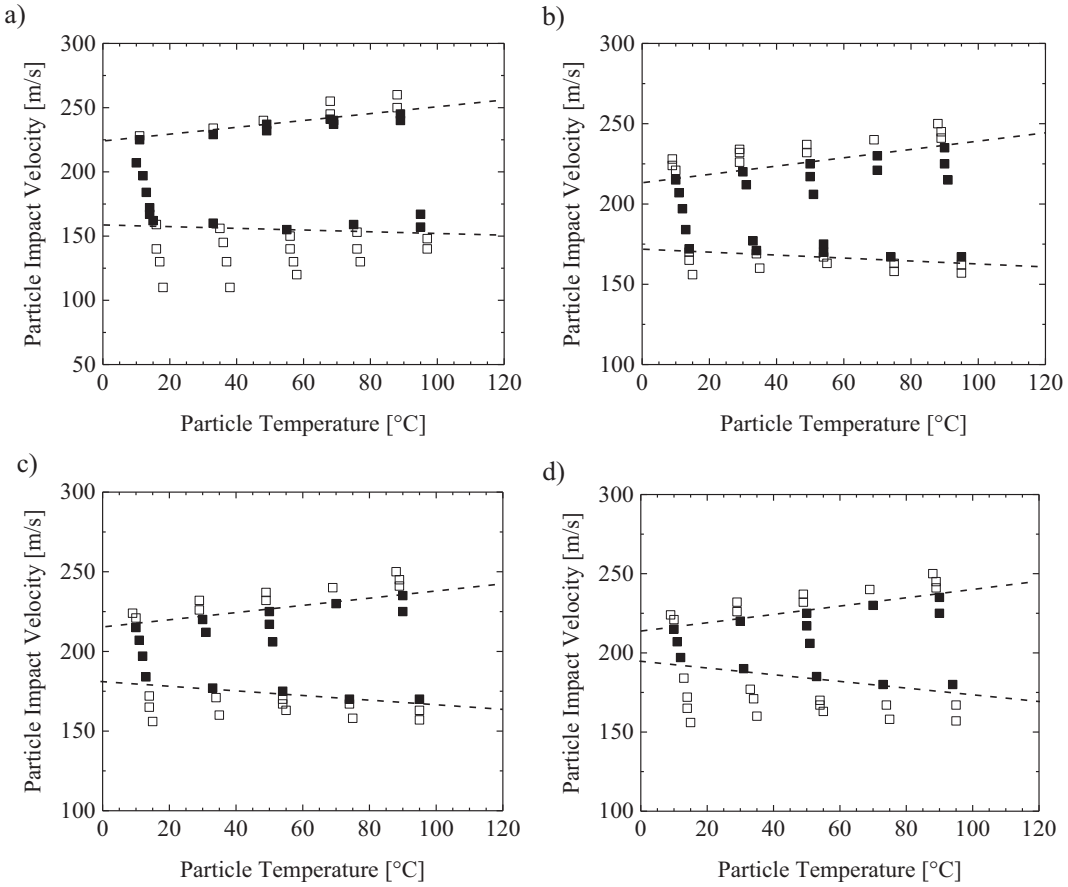

Fig. 5. – Cold spray deposition window of PS particles on (a) LDPE, (b) PS, (c) PVC and (d) POM in cold spray experiment showing the transition from no deposition (▫) to deposition (■). In all cases, the substrate was held fixed at T_s = 100 °C and the nozzle stand-off distance was 10 mm. The dashed lines are not meant to be quantitative but are simply there to guide the reader's eye.

powders, including UHMWPE for which deposition efficiency of 2.9% was achieved at the highest temperatures and impact velocities tested in Fig. 6.

3.2. Deposition efficiency

The cold spray deposition efficiency, *DE*, of all studied particle/substrate pairs for both cases of deposition on LDPE and on melt-cast surfaces of the same polymer are plotted against particle impact velocity in Fig. 7. The change in the mass of the substrate before and after the cold spray process divided by the total amount of sprayed powder was reported as the deposition efficiency. The deposition efficiency of the HDPE particles from Bush et al. [3] is also plotted in Fig. 7. HDPE was found to be significantly larger than all the other polymers tested. Its maximum deposition efficiency was found to be > 8% on LDPE and 5% on a melt-cast surface of HDPE. None of the other polymer tested achieved an efficiency of > 6%. The deposition efficiency of the PU particles was found to be larger than either the PA and

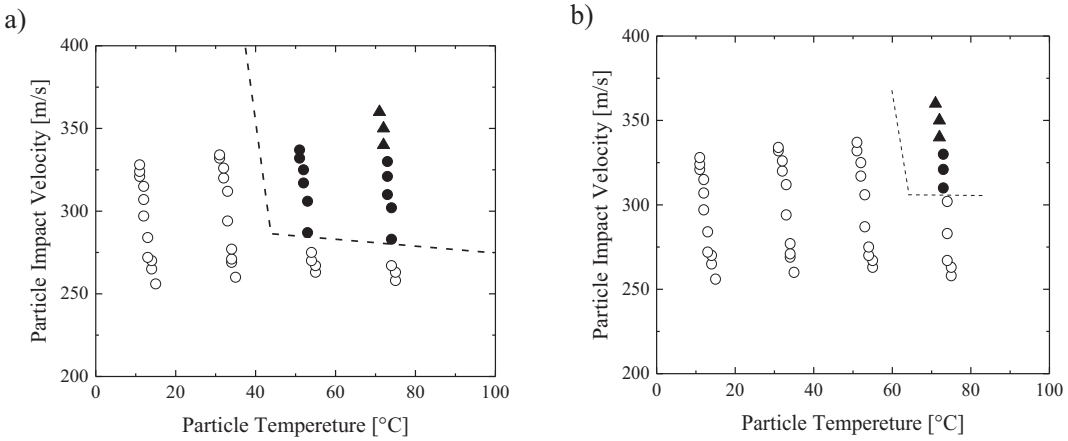

Fig. 6. Cold spray deposition window of UHMWPE particles on (a) LDPE, and (b) UHMWPE showing the transition from no deposition (○) to deposition (●, ▲). The solid triangle symbols (▲) correspond to the results using converging-diverging nozzle to generate supersonic flows. In all cases, the substrate was held fixed at T_s = 100 °C and the nozzle stand-off distance was 10 mm.

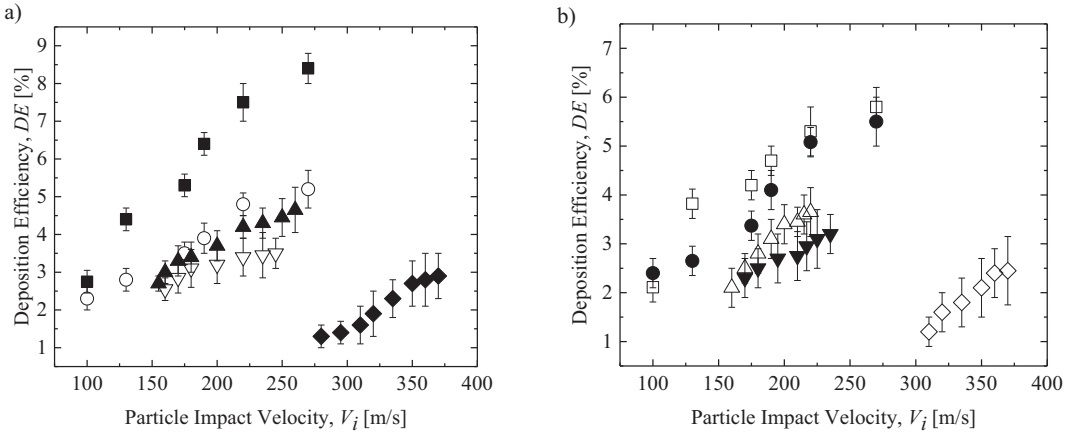

Fig. 7. – Variation of deposition efficiency with the particle impact velocity for both (a) deposition on LDPE and (b) like-on-like depositions in the cold spray experiments. (■, □) HDPE, (●, o) PU, (▲, Δ) PA, (▼, ∇) PS, and (◆, ◊) UHMWPE. Particles of HDPE, PU and UHMWPE were at T_p = 80 °C and PS and PA particles were at T_p = 120 °C. Substrate temperature was kept at T_s = 100 °C for all experiments.

PS particles for both the case of cold spray deposition on LDPE and the case of like-on-like deposition. The deposition efficiency of UHMWPE particles was found to be quite low at < 3%. These differences are likely due to the differences in their glass transition temperatures and variations of their mechanical and viscoelastic properties at elevated temperatures and at these extremely high deformation rates.

In Fig. 7, a monotonic increase in the deposition efficiency is observed with increasing impact velocity for all the particles in both like-on-like deposition cases as well as in cases of deposition on LDPE. With increasing impact velocity, however, the deposition efficiency was not found to increase past 10% for any of the velocities or any of the studied particle-substrate combinations. For metals like copper and aluminum, on the other hand, the variation of deposition efficiency with particle impact velocity is reported to be quite different [7]. The deposition efficiency of metals resembles a step function rather than a continuous trend observed here. In metal cold spray, at impact velocities just above the critical velocity, a deposition efficiency of DE = 25% is observed, but then it abruptly increases to DE = 75–100% at impact velocities higher than $1.2V_{cr}$ [7]. A similar trend was not observed here or for HDPE depositions in the past [3]. Interestingly, for the cases that demonstrate an upper velocity limit in their window of deposition, there is no reduction of deposition efficiency at the highest velocities at which deposition was possible. Instead, the data abruptly goes from a maximum deposition efficiency to DE = 0% for velocities above the maximum critical velocity. This is because at these high velocities, deposition is initially achieved, but due to the poor initial adhesion between the particle and the substrate, large sheets of deposited material are stripped off by the shear stresses generated by high speed gas as the impinging jet is translated across the substrate.

The temperature of both the particles and the substrates were found to play a key role in contributing to the deposition efficiency. For instance, at room temperature ($T_p = T_s$ = 20 °C), a deposition efficiency of DE = 2.1% was achieved for PU particles deposited on an LDPE substrate at the impact velocity of V_i = 270 m/s. As can be seen in Fig. 7, PU particles deposited at the deposition efficiency of DE = 5.2% at the same impact velocity, but particle temperature of T_p = 80 °C and substrate temperature of T_s = 100 °C. This means a 148% increase in the deposition efficiency as a result of a 60 °C increase in particle temperature (from 20 to 80 °C) and a 100 °C increase in the substrate temperature (from 20 to 120 °C). Similar trends were observed for all the polymer powders tested. The maximum deposition efficiency achieved for each polymer substrate combination is presented in Table 2.

Table 2
– Maximum deposition efficiency percentage measured for various particle/substrate pairs under optimized conditions.

Particles substrate	HDPE	PU	PA12	PS	UHMWPE
LDPE	8.4	5.2	4.65	3.5	2.9
HDPE	5.8	–	–	–	–
PU	–	5.5	–	–	–
PA12	–	–	3.65	–	–
PS	–	–	–	3.2	–
UHMWPE	–	–	–	–	2.45

3.3. Deposition properties and SEM studies

Images of a subset of the cold-sprayed coatings of square 2D patterns are presented in Fig. 8. In general, increasing the particle impact velocity and the temperature of either the particle or the substrate was found to slightly increase the buildup thickness due to a corresponding increase in deposition efficiency. Traverse speed was found to be inversely related to the final coating thickness. For example, at a traverse speed of 30 mm/s, HDPE particles were found to build up a 3 mm coating thickness on an LDPE substrate whereas at 40 mm/s traverse speed, only 2 mm thick HDPE coating was built up. Other spray conditions in the later experiment were an impact velocity of 270 m/s, a particle temperature of T_p = 60 °C and substrate temperature of T_s = 100 °C. Under the same spray conditions and the traverse speed of 30 mm/s, a 2.2 mm coating thickness was built up for PU particles and a 1 mm coating thickness was built up for PA and PS. Changing the traverse speed did not result in a visible difference in the thickness of the coatings for PU, PA, and PS particles.

The surface topology of the cold sprayed samples was examined via scanning electron microscopy (SEM) (FEI Magellan 400 XHR-SEM). Several deposition conditions for each of the polymer powders were examined from a top view, 45° tilt angle and 90° tilt angle to view the cross section, investigate porosity of the coatings, and observe the boundary between the substrate and the deposited layer. A small subset of these images is presented in Fig. 9 with arrows superimposed over the cross-sectional images to show the location of the transition from the substrate to the cold spray deposited layer. In all cases, the deposits were quite similar showing little to no porosity and a smooth surface finish with an average surface roughness of < 10 μm without obvious traces of individual powder particles. It is important to emphasize that given that the average size of the particles deposited was between 20 μm and 50 μm, at the magnification of the SEM images, impact craters of unadhered particles or evidence of individual particles should be visible if present. However, no voids or obvious particle boundaries

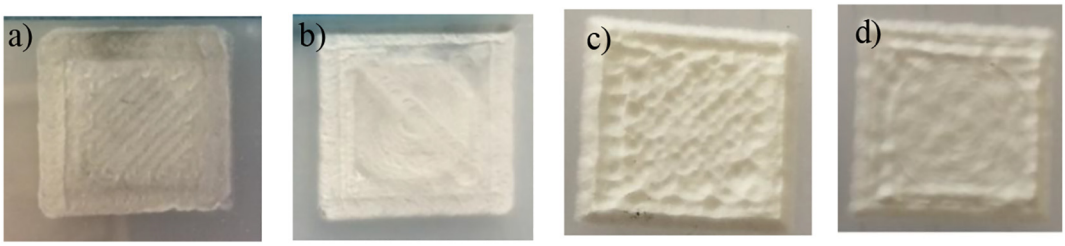

Fig. 8. – Cold-sprayed coatings of square 2D patterns deposited on LDPE. The data includes (a) PU, (b) PA, (c) PS, and (d) UHMWPE.

between individual particles or between individual particles and the substrate could be observed either from the top or cross-sectional views. In fact, in most images, the boundary between the melt cast substrate and the deposited particles is difficult to identify because there is little contrast or obvious microstructural difference between the two layers. One possible explanation for the high quality of the deposition is that, as we will describe in Section 3.3, the deposition efficiencies for all of these powders were found to be < 10%. As a result, the remaining 90% of particles that did not adhere to the substrate may have been responsible for peening the deposition into a dense and smooth coating. < min Additionally, morphology, size, impact angle of each sprayed particle, the unique kinetic and thermal history experienced by each individual particle, whether or not an already deposited particle exists where the incoming particle hits the surface, etc. are also important factors that can affect the dynamics of the sprayed particles upon impacting the substrate.

In Fig. 10, an SEM image of a weakly adhered like-on-like deposition of the PS particle at $V_i = 165$ m/s is shown. This poorly deposited layer was subsequently stripped off the PS melt cast substrate by the high-speed impinging jet of air after being initially deposited. In some cases, like this, the high shear stresses applied to the deposited layer from the airflow and the incoming particles can delaminate on initially deposited layer. The bottom view of a deposited PS layer after being stripped off the melt cast PS substrate is also shown in Fig. 10. The hexagonal structure of the delaminated layer in Fig. 10b clearly shows evidence of individual particles. Under these conditions, the particles deposit to form a close-packed hexagonal lattice upon impacting the substrate. Although some deformation is clear at the boundaries between particles, these particles have not undergone the significant plastic deformation observed in well-adhered and non-porous depositions in Fig. 9. The reduced plastic deformation is likely due to the large glass transition temperature and brittle nature of the PS particles.

Plastic deformation is clearly isolated to areas of high shear formation where temperatures are known to rise significantly, and the particle can soften and perhaps even melt and flow [4]. Subsequent peening from non-adhesive particles clearly does not have as large of an impact in this case because the PS requires significant additional heating to get above its glass transition or even its melt temperature and to flow. At these low velocities and temperature, once a particle has initially adhered to the substrate, it might take multiple impacts in quick succession to peen the particles into a smooth, uniform substrate. This observation may also explain the lower deposition efficiencies observed for PS and other high glass transition temperature polymers.

3.4. Critical angle for deposition

In 3D printing, crack sealing, coating repair and additive manufacturing processes in general, it is worthwhile to define the maximum impact angle at which the sprayed particles deposit on a substrate. Knowing this critical angle will allow for the determination of the feasibility of creating a uniform thin coating that conforms to substrates that are not flat but have surface roughness and/or specific topographical features. In the experiments that follow, the cold-spray nozzle was kept stationary and an LDPE substrate was tilted at angles between $\alpha = 0^\circ$ and $\alpha = 90^\circ$ from the horizontal as shown in Fig. 11. The tilted substrate simulates the conditions of a particle impacting a rough surface either due to its surface finish or the accumulation of previous particles deposited through cold spray. Because a separate tilting stage was used, the printed circuit board plate could not be used to heat the LDPE substrates. As a result, all experiments were performed with a room temperature target substrate. Additionally, the 1D motion of the stage was aligned normal to the tilting direction, so that the stand-off distance was held fixed during stage motion. It is important to note that even for a substrate held perpendicular to the gas/particle stream, cold-sprayed particles impact the substrate at a wide range of impact angles due to the turbulence in the air and the associated turbulent drag forces and due to the collisions with other particles and the walls of the nozzle. On average, the particles move in the direction of the gas flow. As shown in Fig. 12, particles deposit most efficiently when they impact normal to the substrate surface. All samples showed a monotonic decrease in deposition efficiency with increasing substrate tilt angle. Additionally, as seen in Fig. 12, beyond a critical tilt angle, successful deposition was not possible. Increasing the tilt angle reduces the normal component of the impact kinetic energy, $\frac{1}{2}m_p V_i^2 \cos^2\alpha$, available to heat and deform the impacting particle while simultaneously increasing the tangential component of the impact velocity leading to shear stresses that can strip off poorly adhered particles.

In Fig. 13, the maximum tilting angle at which successful cold spray deposition was possible on an LDPE substrate is shown for HDPE, PU, PA and PS particles as a function of both particle temperature and velocity. Results for UHMWPE particles are not presented in Fig. 13 because deposition on a room temperature substrate was not possible. Increasing either particle temperature or impact velocity was found to result in an increase in the maximum tilting angle for substrate. For instance, increasing the PU particle temperature from $T_p = 20$ °C to 80 °C resulted in an increase in the maximum substrate tilt angle from 20° to 60°. Similar increases were observed for the other particles with temperature and velocity increases from $V_i = 150$ m/s to 300 m/s. This trend can be explained by considering the normal component of the impact velocity, $V_i \cos\alpha$, which is plotted in Fig. 14, for the four polymer particles studied. For the low-T_g particles, HDPE and PU, the minimum normal component of the impact velocity needed for successful deposition, $V_i \cos\alpha_{max}$, remains roughly constant at between 150 m/s and 160 m/s over the entire range of impact velocities. Note that this value correlates precisely with the velocity corresponds nearly perfectly with the critical impact velocity for HDPE and PU when the tilt angle is at $\alpha = 0^\circ$, which was found to be $V_{crit} = 150$ m/s and 160 m/s, respectively. These results suggest that only the normal component of the velocity is important in particle adhesion. For the high-T_g polymers, PA and PS, however, the results are not as cut and dry. For PA and PS, the minimum normal component of the impact velocity needed for successful deposition, $V_i \cos\alpha_{max}$, was found to grows slowly from approximately 170 to 210 m/s with increasing particle impact velocity. The low velocity limit is in agreement with the results for $\alpha = 0^\circ$, but it appears to become increasingly more difficult to deposit high-T_g particles on a substrate as the tilt angle is increased. This observed increase in the normal component of the critical impact velocity might be due to the increase in shear stress from the air flow

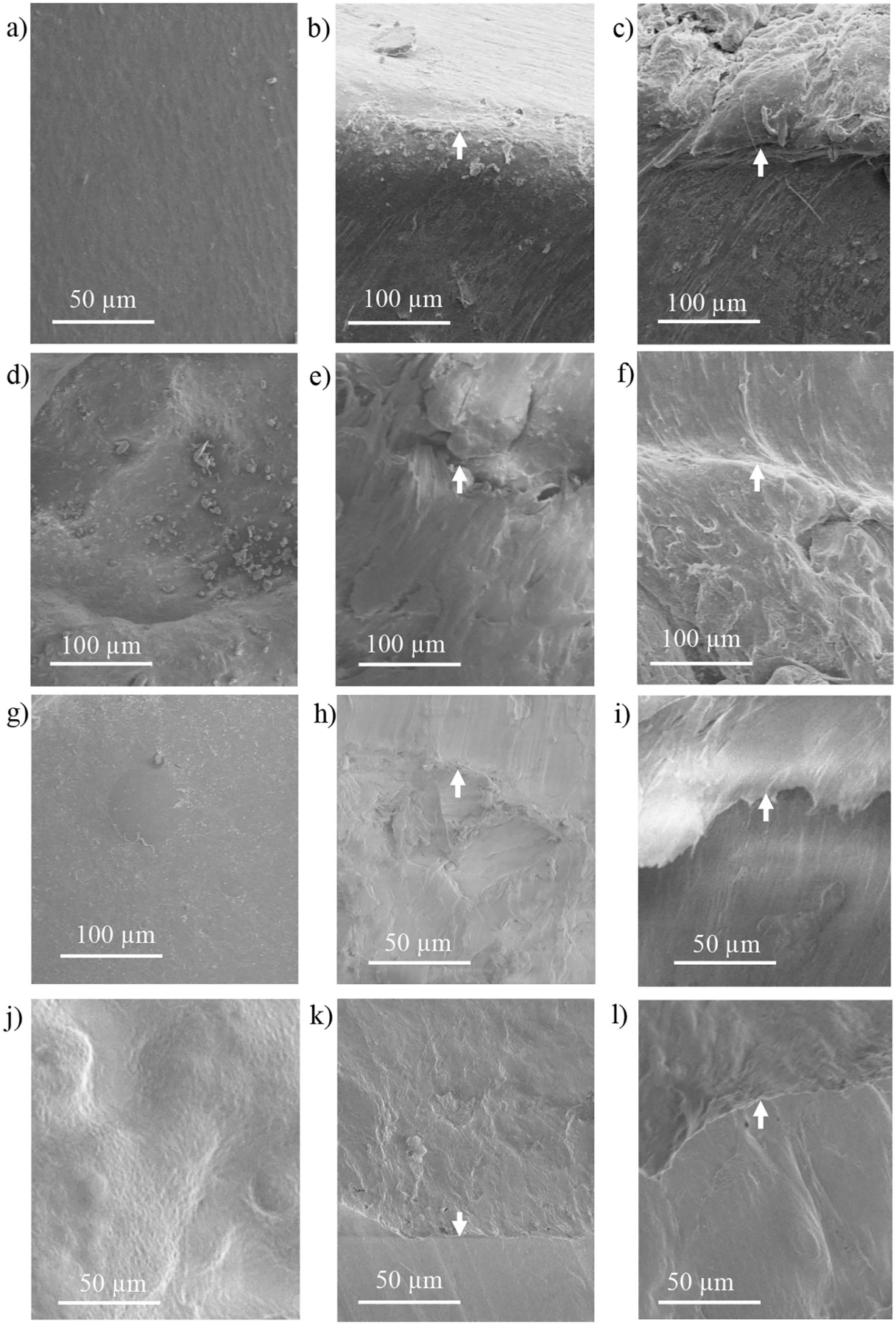

(caption on next page)

Fig. 9. SEM imaging of cold-sprayed deposits of (a, b, c) PU, (d, e, f) PA, (g, h, i) PS, and (j, K, l) UHMWPE. In each row, the sequence of the images is the top view, cross-sectional view of the deposited particles on LDPE and cross-sectional view for the like-on-like deposition. Cold spray parameters included $T_p = 20\,^{\circ}C$ and $V_i = 130$ m/s for PU, $T_p = 20\,^{\circ}C$ and $V_i = 170$ m/s for PA, $T_p = 20\,^{\circ}C$ and $V_i = 200$ m/s for PS, and $T_p = 80\,^{\circ}C$ and $V_i = 310$ m/s for UHMWPE. In the cross-section views, an arrow is used to indicate the boundary between melt-cast (bottom) and cold-sprayed (top) polymer.

and glancing collisions from non-adhesive particles with increasing gas flow velocity and substrate angle. This is more obvious for the high-T_g polymers, for which single particle impact experiments have demonstrated that upon impact high-T_g particles undergo significantly less deformation [4] than the low-T_g particles [43]. As a result, high-T_g particles are less strongly adhered upon initial deposition and more susceptible to being removed by shear stress from the gas or collisions.

These tilt angle experiments, suggest that, if the traverse speed is slow enough, a 1D line deposited using cold spray should obtain a triangular cross section with a side angle that corresponds to the critical deposition angle at the operating condition being used. These triangular cross-sections have in fact been observed here, as shown in Fig. 15, and were documented previously by Bush et al. [3]. These results also suggest, that a minimum traverse speed is needed to efficiently deposit polymer particles because once the triangular cross-section has been deposited with a base width of the impinging jet diameter, no additional deposition is possible. So, if the traverse speed is too slow, the overall deposition efficiency will reduce because of the existence of a maximum deposition angle. There is thus an optimal particle flow rate and substrate traverse speed that should optimize deposition efficiency. Take for example the deposition of HDPE particles on an LDPE substrate. As the traverse speed was increased by a factor of two, from 15 to 30 mm/s, the deposition efficiency was found to increase from 6.5% to 9% for an impact velocity of $V_i = 250$ m/s and a particle temperature of $T_p = 80\,^{\circ}C$. The coating thickness was simultaneously reduced by only 20% even as the speed was doubled. Increasing the traverse speed beyond 30 mm/s did not result in further improvements in deposition efficiency as images of the cross sectional profile revealed a more rounded profile than the triangular profile seen at 15 mm/s. This result suggests that surface roughness and the topography of the deposited layer can play a large role in the overall deposition efficiency. Further understanding the role of surface topography should lead to even higher deposition efficiency in the future.

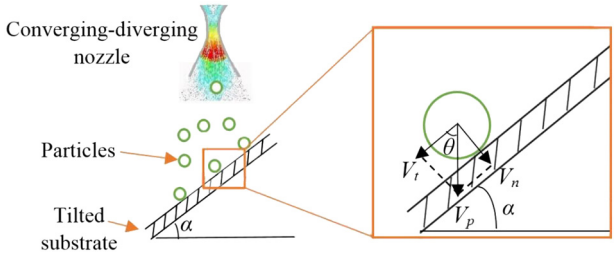

Fig. 11. Schematic diagram of cold sprayed particles impacting a tilted substrate.

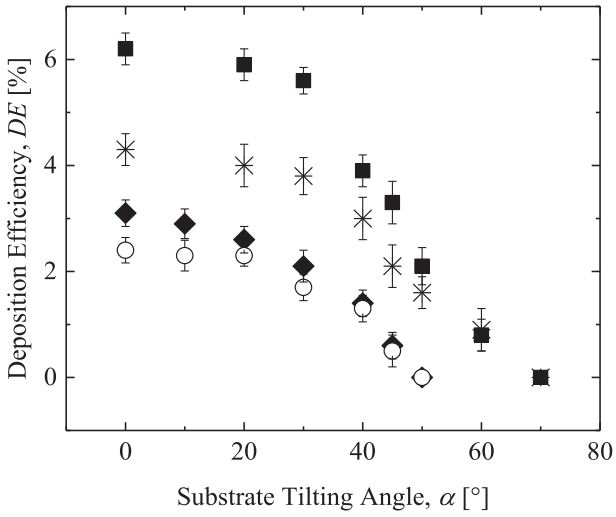

Fig. 12. Deposition efficiency as a function of the tilt angle of the substrate for a particle impact velocity of $V_i = 280$ m/s, a the particle temperature was kept at $T_p = 50\,^{\circ}C$ and a room temperature substrate for a standoff distance of 10 mm. The data include: (■) HDPE, (*) PU, (♦) PA, and (○) PS.

3.5. Characterization of mechanical properties of the cold-sprayed coatings

3.5.1. Nano-hardness

As described in the materials and methods section, nano-indentation measurements were performed to measure the hardness of the cold-sprayed coatings and to compare them to the melt-cast coatings. A trapezoidal loading function with 5 s peek holding time and 5 s for loading/unloading was used for all experiments. The loading and its corresponding displacement were recorded as a function of time during the experiment. For each test, the procedure was repeated 20 times in various positions and the average value along with its standard deviation is reported in Table 3. Comparing the nano-hardness of the cold-sprayed samples and those of the melt cast samples in Table 3, a remarkable consistency between the values of nano-hardness can be observed for each of the materials studied. A general reduction of 5–10% was observed for most cold sprayed samples. However, this variation

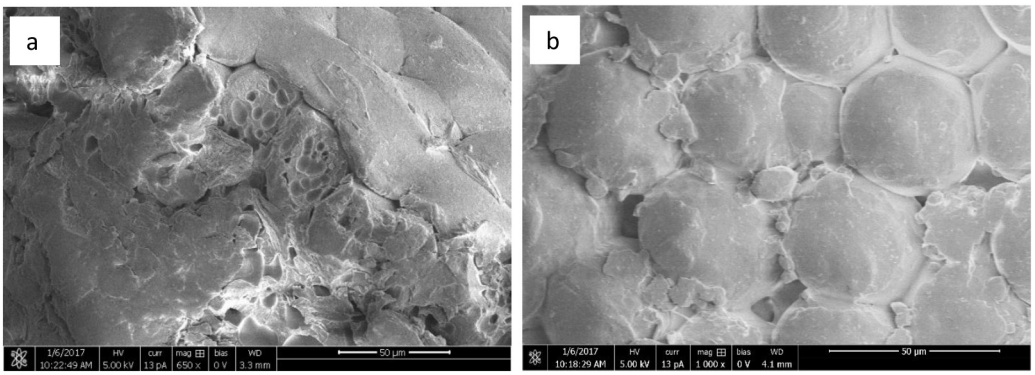

Fig. 10. SEM imaging of a poorly deposited PS on a melt cast PS substrate showing (a) the cross section and (b) bottom view after the delamination of the deposited layer. This surface was deposited at $V_i = 165$ m/s and $T_p = 20\,^{\circ}C$.

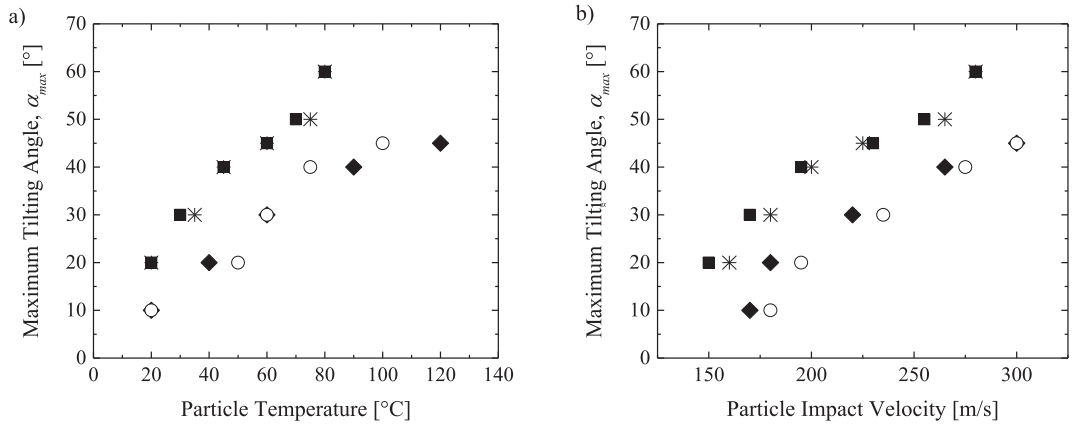

Fig. 13. Maximum tilting angle for successful deposition on an LDPE substrate as a function of (a) particle temperature and (b) impact velocity. The particle impact velocity was V_i = 190 m/s for all the experiments in (a) and the particle temperature was kept at T_p = 50 °C for all experiments in (b). The substrate was at room temperature and the standoff distance was kept at 10 mm. The data include: (■) HDPE, (*) PU, (♦) PA, and (○) PS.

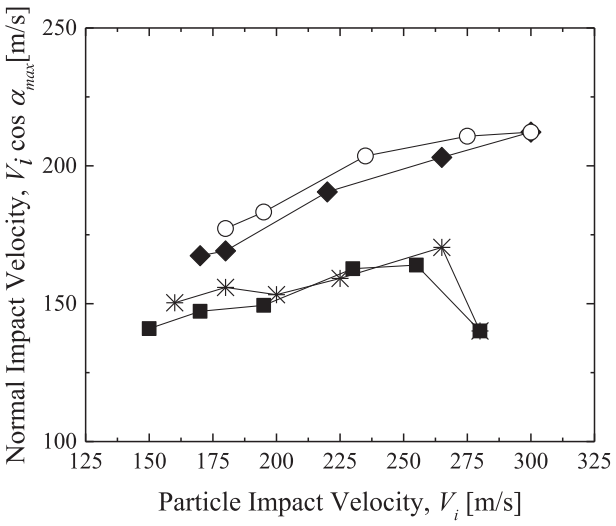

Fig. 14. Normal component of the critical particle impact velocity, $V_i \cos \alpha_{max}$, at the maximum substrate tilt angles for successful deposition on LDPE as a function of the measured critical particle impact velocity. In all cases, the substrate was maintained at room temperature and the particles were at T_p = 50 °C. The data include: (■) HDPE, (*) PU, (♦) PA, and (○) PS.

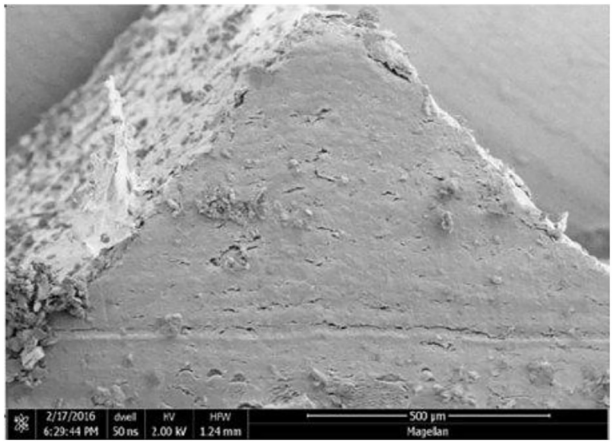

Fig. 15. The triangular cross-section of a deposited line of HDPE particles on an LDPE substrate at a traverse speed of 15 mm/s, particle impact velocity of 200 m/s, T_P = 80 °C, and T_S = 100 °C.

Table 3
– Nano-hardness of the cold-sprayed coatings in comparison to the melt cast samples.

	Nano-hardness (MPa)	
	Melt cast	Cold sprayed
LDPE	210 ± 10	–
HDPE	260 ± 20	220 ± 20
PU	200 ± 20	200 ± 20
PS	390 ± 20	380 ± 20
PA	270 ± 20	260 ± 20

does not appear to be significant as it is within the experimental uncertainty. The values obtained are consistent with reported values in the literature.

3.5.2. Adhesion/Cohesion strength

As described in Section 2, tensile test samples were prepared with the coating/substrate layer glued to the middle of a standard dog bone following the ASTM - C633 standard protocol to investigate the adhesion strength of the cold-spray deposited layer. Rectangular prisms of coating/substrate pairs were prepared of each of the five polymer materials studied in this work, HDPE, PU, PA, PS, and UHMPE. The coating and substrate materials forming the rectangular prism were identical in each sample. The only difference was whether the coating was cold sprayed or melt-cast. The rectangular prisms of each coating/substrate pairs were then glued between the two halves of a dog-bone sample of melt-cast polyamide 12 as shown in Fig. 2. Five more pure dog bone samples were melt-cast of each of the five polymer materials to be tested and compared to those with the rectangular prism attached in the middle. Stress/strain curves for each of the polymer powders tested here are presented in Fig. 16. The hollow symbols in Fig. 16, represent the results for dog bones with the rectangular prism attached in the middle. The solid symbols in this figure refer to the results from pure dog bone samples made of melt-cast polymers.

The linear, small strain data in Fig. 16 was used to calculate the Young modulus presented in Table 4. All the materials tested in this study exhibited a cohesive failure with the fracture occurring within the cold sprayed coating. These studies confirm the high adhesive strength between the cold-sprayed particles and the melt-cast substrate.

The scatter between multiple repeated test results in Fig. 16, was small and a quantitative agreement was achieved between the tensile tests of the cold sprayed samples and the melt-cast specimens of the same material. Analyzing these curves in more detail can provide insight in how the deposition technique can affect the solid-state

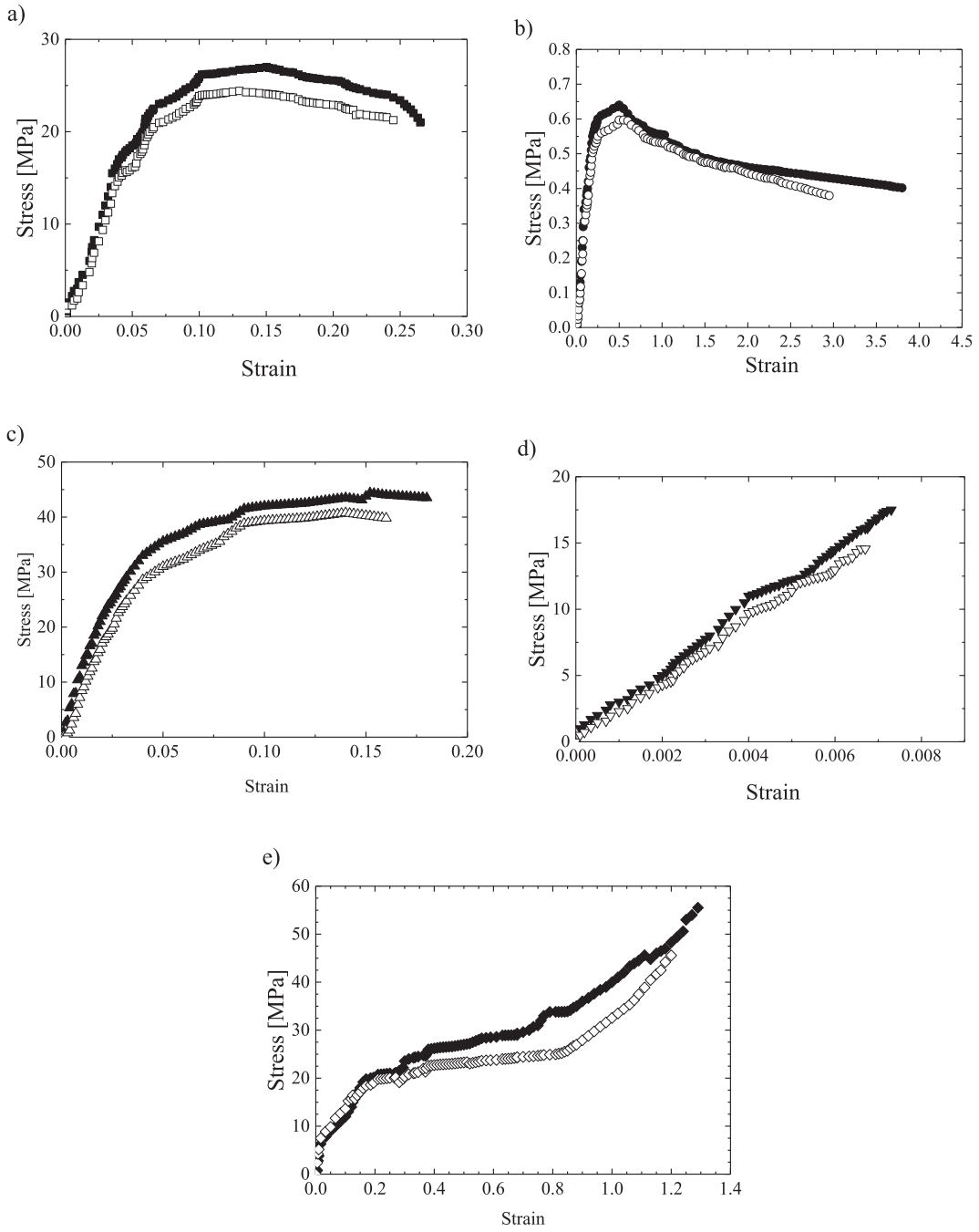

Fig. 16. Stress-strain curves produced from tensile testing until failure of (a) HDPE, (b) PU, (c) PA, (d) PS, (e) UHMWPE. Data for melt-cast samples are represented by solid symbols and cold sprayed samples by hollow symbols.

Table 4
Mechanical properties including ultimate tensile strength (UTS), elongation at failure, Young's modulus, and fracture toughness for both like-on-like cold-sprayed samples and the corresponding melt-cast samples.

		UTS [MPa]	Elongation at failure	Young's Modulus [GPa]	Toughness [MPa]
HDPE	Cold sprayed	24 ± 4	0.25 ± 0.06	0.29 ± 0.05	5.4 ± 0.1
	Melt-cast	27 ± 3	0.27 ± 0.05	0.32 ± 0.04	5.8 ± 0.2
PU	Cold sprayed	0.59 ± 0.03	3.0 ± 0.1	0.0034 ± 0.0001	1.9 ± 0.2
	Melt-cast	0.64 ± 0.03	3.8 ± 0.08	0.0037 ± 0.0002	2.0 ± 0.4
PA	Cold sprayed	40 ± 4	0.16 ± 0.05	1.1 ± 0.1	5.8 ± 0.1
	Melt-cast	43 ± 3	0.18 ± 0.05	1.3 ± 0.1	6.1 ± 0.3
PS	Cold sprayed	14.6 ± 0.8	0.007 ± 0.003	2.0 ± 0.1	0.062 ± 0.003
	Melt-cast	18 ± 1	0.073 ± 0.001	2.1 ± 0.1	0.068 ± 0.005
UHMWPE	Cold sprayed	46 ± 8	1.2 ± 0.2	0.63 ± 0.09	27 ± 6
	Melt-cast	60 ± 5	1.3 ± 0.2	0.66 ± 0.07	32 ± 8

properties of a coating. From Table 4, little difference can be observed between the cold-sprayed and melt-cast samples in their Young's modulus, ultimate tensile strength (UTS), elongation at failure, or toughness. Cold spraying polymer powder does not embrittle a coating, as evident in the lack of variation in the elongation at failure. This is true even though impact-induced stresses are likely frozen in during deposition. Residual stresses either appear to be small enough not to affect the polymer ductility or perhaps they have been worked out through the peening of subsequent, non-adhering particles. No statistically significant deviation in the toughness of cold-sprayed samples was observed. This is especially important for the UHMWPE samples as its enhanced toughness is one of its more desirable characteristics. Here the cold-sprayed UHMWPE sample showed a modest decrease in toughness although the change was well within the uncertainty of the data and as a result it should not be considered significant.

4. Conclusions

Cold spray deposition of HDPE, PU, PA, PS and UHMWPE were found to be feasible on polymeric substrates. Deposition windows developed for a variety of particle/substrate combinations revealed that the critical velocity decreased while the upper-limit velocity (if any) increased, as the temperature increased. SEM studies confirmed that the depositions were without defect and had low porosity, once the spray conditions were optimized. Mechanical properties including nanohardness, elastic modulus, ultimate tensile strength, elongation at break, and fracture toughness were measured and found to be roughly the same for the cold-sprayed samples and the corresponding melt-cast specimens. All cold sprayed samples showed cohesive failure, demonstrating strong adhesion between the cold-sprayed polymer and the melt-cast substrate. A critical angle beyond which tilting the substrate made deposition impossible was found as a function of deposition conditions. These measurements suggested only the normal component of the impact velocity was important in deposition. These measurements also suggested that conformal coatings of topographically complex surfaces are possible opening up the possibility of using cold spray deposition of polymers as a new technique for 3D additive manufacturing of parts.

Author contribution

This study was implemented by Zahra Khalkhali and supervised by Professor Jonathan P. Rothstein as a PhD project.

Declaration of competing interest

The authors declare that they have no known competing financial interests or personal relationships that could have appeared to influence the work reported in this paper.

Acknowledgments

This research was accomplished through a cooperative research agreement with the US Army Research Laboratory, Contract: W911NF-15-2-0024, P00003 ‘Intelligent Processing of Materials by Design.’

References

[1] A. Papyrin, V. Kosarev, S. Klinkov, A. Alkhimov, V.M. Fomin, Cold Spray Technology, Elsevier, Amsterdam, 2007.
[2] F.S. da Silva, N. Cinca, S. Dosta, I.G. Cano, J.M. Guilemany, C.S.A. Caires, A.R. Lima, C.M. Silva, S.L. Oliveira, A.R.L. Caires, A.V. Benedetti, Corrosion resistance and antibacterial properties of copper coating deposited by cold gas spray, Surf. Coat. Technol. 361 (2019) 292–301.
[3] T.P. Bush, Z. Khalkhali, V.K. Champagne, D.P. Schmidt, J.P. Rothstein, Optimization of cold spray deposition of high-density polyethylene powders, Thermal Spray Technology 26 (7) (2017) 1548–1564.
[4] Z. Khalkhali, W. Xie, V.K. Champagne, J.-H. Lee, J.P. Rothstein, A comparison of cold spray technique to single particle micro-ballistic impacts for the deposition of polymer particles on polymer substrates, Surface & Coatings Technology 351 (2018) 99–107.
[5] A. Astarita, L. Boccarusso, M. Durante, A. Viscusi, R. Sansone, L. Carrino, Study of the production of a metallic coating on natural Fiber composite through the cold spray technique, Materials Engineering Performance 27 (2) (2018) 739–750.
[6] G. Archambault, B. Jodoin, S. Gaydos, M. Yandouzi, Metallization of carbon fiber reinforced polymer composite by cold spray and lay-up molding processes, Surafce and Coating Technology 300 (2016) 78–86.
[7] H. Assadi, T. Schmidt, H. Richter, J.-O. Kliemann, K. Binder, F. Gartner, T. Klassen, H. Kreye, On parameter selection in cold spraying, J. Therm. Spray Technol. 20 (6) (2011) 1161–1176.
[8] M. Gardon, A. Latorre, M. Torrell, S. Dosta, J. Fernandez, J.M. Guilemany, Cold gas spray titanium coatings onto a biocompatible polymer, Mater. Lett. 106 (2013) 97–99.
[9] F. Robitaille, M. Yandouzi, S. Hind, B. Jodoin, Metallic coating of aerospace carbon/epoxy composites by the pulsed gas dynamic spraying process, Surf. Coat. Technol. 203 (19) (2009) 2954–2960.
[10] J. Affi, H. Okazaki, M. Yamada, M. Fukumoto, Fabrication of aluminum coating onto CFRP substrate by cold spray, Mater. Trans. 52 (9) (2011) 1759–1763.
[11] P.S.M. Rajesh, F. Sirois, D. Therriault, Damage response of composites coated with conducting materials subjected to emulated lightning strikes, Mater. Des. 139 (2018) 45–55.
[12] H. Che, M. Gagne, P.S.M. Rajesh, J.E. Sapieha, F. Sirois, D. Therriault, S. Yue, Metallization of carbon fibre reinforced polymer for lightning strike protection, Materials Engineering Performance 27 (10) (2018) 5205–5211.
[13] A.M. Vilardell, N. Cinca, A. Concustell, S. Dosta, I.G. Cano, J.M. Guilemany, Cold spray as an emerging technology for biocompatible and antibacterial coatings: state of art, Mater. Sci. 50 (2015) 4441–4462.
[14] X. Zhou, P. Mohanty, Electrochemical behavior of cold sprayed hydroxyapatite/titanium composite in Hanks' solution, Electrochim. Acta 65 (2012) 134–140.
[15] N. Cinca, A.M. Vilardell, S. Dosta, A. Concustell, I. Garcia Cano, J.M. Guilemany, S. Estrade, A. Ruiz, F. Peiro, A new alternative for obtaining nanocrystalline bioactive coatings: study of hydroxyapatite deposition mechanisms by cold gas spraying, American Ceramic Society 99 (2016) 1420–1428.
[16] M. Robotti, S. Dosta, C. Fernandez-Rodriguez, M.J. Hernandez-Rodriguez, I.G. Cano, E.P. Melian, J.M. Guilemany, Photocatalytic abatement of NOx by CTiO2/polymer composite coatings obtained by low pressure cold gas spraying, Appl. Surf. Sci. 362 (2016) 274–280.
[17] L. Wang, F. Wang, S. Li, Y. Wang, Microstructure and application of alumina-supported cu-based coating prepared by cold spray, Surface & Coatings Technology 362 (2019) 113–123.
[18] M.J. Vucko, P.C. King, A.J. Poole, Y. Hu, M.Z. Jahedi, R. de Nys, Assessing the antifouling properties of cold-spray metal embedment using loading density gradients of metal particles, Biofouling 30 (2014) 651–666.
[19] C. Stenson, K.A. McDonnell, S. Yin, B. Aldwell, M. Meyer, D.P. Dowling, R. Lupoi, Cold spray deposition to prevent fouling of polymer surfaces, Surf. Eng. 34 (3) (2018) 1–11.
[20] P.A. Podrabinnik, I.V. Shishkovsky, Laser post annealing of cold-sprayed Al–Ni composite coatings for green energy tasks, Procedia IUTAM 23 (2017) 108–113.
[21] G. Yang, W. Xie, M. Huang, V.K. Champagne, J.-H. Lee, J. Klier, J.D. Schiffman, Polymer particles with a low glass transition temperature containing Termoset resin enable powder coatings at room temperature, Ind. Eng. Chem. Res. 58 (2019) 908–916.
[22] T. Hussain, Cold spraying of titanium: a review of bonding mechanisms, microstructure and properties, Key Eng. Mater. 533 (2013) 53–90.
[23] H. Assadi, F. Gartner, T. Stoltenhoff, H. Kreye, Bonding mechanism in cold gas spraying, Acta Mater. 51 (2003) 4379–4394.
[24] M. Grujicic, J.R. Saylor, D.E. Beasley, W.S. DeRosset, D. Helfritch, Computational analysis of the interfacial bonding between feed-powder particles and the substrate in the cold-gas dynamic-spray process, Appl. Surf. Sci. 219 (2003) 211–227.
[25] X.L. Zhou, A.F. Chen, J.C. Liu, X.K. Wu, J.S. Zhang, Preparation of metallic coatings on polymer matrix composites by cold spray, Surface & Coating Technology 206 (1) (2011) 132–136.
[26] H. Che, P. Vo, S. Yue, Metallization of carbon fibre reinforced polymers by cold spray, Surf. Coat. Technol. 313 (2017) 236–247.
[27] Mostafa Hassani-Gangaraj, David Veysset, Victor K. Champagne, Keith A. Nelson, Christopher A. Schuh, Adiabatic shear instability is not necessary for adhesion in cold spray, Acta Mater. 158 (2018) 430–439.
[28] S.I. Imbriglio, M. Hassani-Gangaraj, D. Veysset, M. Aghasibeig, R. Gauvin, K.A. Nelson, C.A. Schuh, R.R. Chromik, Adhesion strength of titanium particles to alumina substrates: a combined cold spray and LIPIT study, Surface & Coatings Technology 361 (2019) 403–412.
[29] Y. Xu, I.M. Hutchings, Cold spray deposition of thermoplastic powder, Surf. Coat. Technol. 201 (6) (2006) 3044–3050.
[30] S. Shah, J. Lee, J.P. Rothstein, Numerical simulations of the high velocity impact of a single polymer particle during cold spray deposition, J. Therm. Spray Technol. 26 (5) (2017) 970–984.
[31] A.S. Alhulaifi, G.A. Buck, W.J. Arbegast, Numerical and experimental investigation of cold spray gas dynamic effects for polymer coating, J. Therm. Spray Technol. 21 (2012) 852–862.
[32] K. Ravi, Y. Ichikawa, T. Deplancke, K. Ogawa, O. Lame, J.-Y. Cavaille, Development of Ultra-High Molecular Weight Polyethylene (UHMWPE) coating by cold spray technique, J. Therm. Spray Technol. 24 (6) (2015) 1015–1025.
[33] V. Gillet, E. Aubignat, S. Costil, B. Courant, C. Langlade, P. Casari, W. Knapp, M.P. Planche, Development of low pressure cold sprayed copper coatings on carbon

fiber reinforced polymer (CFRP), Surf. Coat. Technol. 364 (2019) 306–316.
[34] X. Wang, F. Feng, M.A. Klecka, M.D. Mordasky, J.K. Garofano, T. El-Wardany, A. Nardi, V.K. Champagne, Characterization and modeling of the bonding process in cold spray additive manufacturing, Additive Manufacturing 8 (2015) 149–162.
[35] L. Verbelen, S. Dadbakhsh, M. Van de Eynde, J.-P. Kruth, B. Goderis, P. Van Puyvelde, Characterization of polyamide powders for determinationof laser sintering processability, Eur. Poly. J 75 (2016) 163–174.
[36] A. Shapiro, The Dynamics and Thermodynamics of Compressible Fluid Flow, The Ronald Press Company, 1953.
[37] V.K. Champagne, D.J. Helfritch, S.P.G. Dinavahi, P.F. Leyman, Theoretical and experimental particle velocity in cold spray, Thermal Spray Technology 20 (2011) 425–431.
[38] Standard test method for adhesion or cohesion strength of thermal spray coatings, Annual Book of ASTM Standards, vol. C633, ASTM, 2013, p. 8.
[39] K. Petrackova, J. Konda, M. Guagliano, Mechanical performance of cold-sprayed A357 aluminum alloy coatings for repair and additive manufacturing, Thermal Spray Technology 26 (2017) 1888–1897.
[40] T. Schmidt, F. Gartner, H. Assadi, H. Kreye, Development of a generalized parameter window for cold spray deposition, Acta Mater. 54 (2006) 729–742.
[41] H. Suzuki, J. Grebowicz, B. Wunderlich, The glass transition of Polyoxymethylene, British Polymer Journal 17 (1) (1985) 1–3.
[42] K. Ravi, T. Deplancke, K. Ogawa, J.-Y. Cavaille, O. Lame, Understanding deposition mechanism in cold sprayed ultra high molecular weight polyethylene coatings on metals by isolated particle deposition method, Additive Manufacturing 21 (2018) 191–200.
[43] Z. Khalkhali, W. Xie, J.-H. Lee, J.P. Rothstein, Cold Spray Deposition and Laser-Induced Single Particle Impact Experiments for Low Glass Transition Temperature Polymer Particles, Submitted (2019).